Chirped dissipative soliton absorption spectroscopy

Vladimir L. Kalashnikov,[1,*] **Evgeni Sorokin,**[1] **and Irina T. Sorokina**[2]

[1]*Institut für Photonik, TU Wien, Gusshausstrasse 27/387, A-1040 Vienna, Austria*
[2]*Physics Department, Norwegian University of Science and Technology (NTNU), Realfagbygget, Høgskoleringen 5, 7034 Trondheim, Norway*
[*]*kalashnikov@tuwien.ac.at*

http://info.tuwien.ac.at/kalashnikov

Abstract: We present analytical theory of dissipative soliton absorption spectroscopy. A dissipative soliton formed in an all-normal-dispersion oscillator with a narrowband intracavity absorber acquires spectral features that follow the index of refraction of the absorber, as confirmed by numerical simulations and experimental evidence. In contrast to the soliton absorption spectroscopy in an anomalous dispersion regime, we anticipate resonant enhancement of a modulation signal near the pulse spectrum edges that results in an additional signal gain. We further show that the pulse acquires a nanosecond-long tail in the time domain and provide simple formula for estimation of its energy content.

OCIS codes: (140.7090) Ultrafast lasers; (190.5530) Pulse propagation and temporal solitons; (300.6360) Spectroscopy, laser.

References and links

1. V. M. Baev, T. Latz, and P. E. Toschek, "Laser intracavity absorption spectroscopy," Appl. Phys. B **69,** 171 (1999).
2. V. A. Akimov, V. I. Kozlovskii, Yu. V. Korostelin, A. I. Landman, Yu. P. Podmar'kov, and M. P. Frolov, "Spectral dynamics of intracavity absorption in a pulsed Cr^{2+}:ZnSe laser," Quantum Electron. **35,** 425–428 (2005).
3. E. Sorokin, I. T. Sorokina, J. Mandon, G. Guelachvili, and N. Picqué, "Sensitive multiplex spectroscopy in the molecular fingerprint 2.4 μm region with a Cr^{2+}:ZnSe femtosecond laser," Opt. Express **15,** 16540–16545 (2007).
4. *Mid-Infrared Coherent Sources and Applications*, M. Ebrahim-Zadeh, I. T. Sorokina, Eds. (Springer-Verlag, 2008).
5. V. A. Akimov, A. A. Voronov, V. I. Kozlovskii, Yu. V. Korostelin, A. I. Landman, Yu. P. Podmar'kov, and M. P. Frolov, "Intracavity laser spectroscopy by using a Fe^{2+}:ZnSe laser," Quantum Electron. **37,** 1071–1075 (2007).
6. I. T. Sorokina, E. Sorokin, and T. Carrig, "Femtosecond pulse generation from a SESAM mode-locked cr:znse laser," in Conference on Lasers and Electro-Optics/Quantum Electronics and Laser Science Conference and Photonic Applications Systems Technologies, Technical Digest (CD) (Optical Society of America, 2006), paper CMQ2.
7. R. Böhm, A. Stephani, V. M. Baev, and P. E. Toschek, "Intracavity absorption spectroscopy with a Nd^{3+}-doped fiber laser," Opt. Lett. **18,** 1955–1957 (1993).
8. Yu. O. Barmenkov, A. Ortigosa-Blanch, A. Diez, J. L. Cruz, and M. V. Andrés, "Time-domain fiber laser hydrogen sensor," Opt. Lett. **29,** 2461–2463 (2004).
9. A. Starka, L. Correiaa, M. Teichmanna, S. Salewskia, C. Larsenb, V. M. Baev, and P. E. Toscheka, "Intracavity absorption spectroscopy with thulium-doped fibre laser," Opt. Commun. **215,** 113–123 (2003).
10. J. Mandon, G. Guelachvili, E. Sorokin, I. T. Sorokina, V. L. Kalashnikov, and N. Picqué, "Enhancement of molecular dispersion spectral signatures in mode-locked lasers," in EPS-QEOD Europhoton Conference on Solid-state, Fiber and Waveguide Light Sources, Abstract Volume 32G (CD) (Paris, France, 2008), paper WEoB.4.

#149532 - $15.00 USD Received 20 Jun 2011; revised 28 Jul 2011; accepted 5 Aug 2011; published 22 Aug 2011

11. V. L. Kalashnikov, E. Sorokin, J. Mandon, N. Picqué, G. Guelachvili, and I. T. Sorokina, "Femtosecond lasers for intracavity molecular spectroscopy," in EPS-QEOD Europhoton Conference on Solid-state, Fiber and Waveguide Light Sources, Abstract Volume 32G (CD) (Paris, France, 2008), paper TUoA.3.
12. J. Mandon, G. Guelachvili, and N. Picqué, "Fourier transform spectroscopy with a laser frequency comb," Nat. Photonics **3,** 99–102 (2009).
13. V. L. Kalashnikov and E. Sorokin, "Soliton absorption spectroscopy," Phys. Rev. A **81**, 033840 (2010).
14. A. Fernandez, T. Fuji, A. Poppe, A. Fürbach, F. Krausz, and A. Apolonski, "Chirped-pulse oscillators: a route to high-power femtosecond pulses without external amplification," Opt. Lett. **29**, 1366–1368 (2004).
15. A. Chong, J. Buckley, W. Renninger, and F. Wise, "All-normal-dispersion femtoseond fiber laser," Opt. Express **14**, 10095–10100 (2006).
16. V. L. Kalashnikov, "Chirped dissipative solitons," *Nonlinear Dynamics and Applications*, vol. 16, L. F. Babichev, V. I. Kuvshinov, Eds., pp. 58–67 (Minsk, 2010) (also arXiv:1001.4918 [physics.optics]).
17. N. N. Akhmediev and A. Ankiewicz, *Solitons: Nonlinear Pulses and Beams* (Chapman and Hall, 1997).
18. E. Podivilov and V. L. Kalashnikov, "Heavily-chirped solitary pulses in the normal dispersion region: new solutions of the cubic-quintic complex Ginzburg-Landau equation," JETP Lett. **82**, 467–471 (2005).
19. V. L. Kalashnikov, E. Podivilov, A. Chernykh, and A. Apolonski, "Chirped-pulse oscillators: theory and experiment," Appl. Phys. B **83**, 503–510 (2006).
20. V. L. Kalashnikov, Maple 13 computer algebra worksheet, `http://info.tuwien.ac.at/kalashnikov/NCGLE1.html`
21. V. L. Kalashnikov, Maple 14 computer algebra worksheet, `http://info.tuwien.ac.at/kalashnikov/perturb2.html`
22. V. L. Kalashnikov, "Chirped dissipative solitons of the complex cubic-quintic nonlinear Ginzburg-Landau equation," Phys. Rev. E **80**, 046606 (2009).
23. V. L. Kalashnikov and A. Chernykh, "Spectral anomalies and stability of chirped-pulse oscillators," Phys. Rev. A **75**, 033820 (2007).
24. V. L. Kalashnikov, "Dissipative solitons: perturbations and chaos formation," *Chaos Theory. Modeling, Simulation and Applications: Selected Papers from the 3rd Chaotic Modeling and Simulation International Conference (CHAOS2010)*, Ch.H.Skiadas, I.Dimotikalis, Ch.Skiadas, Eds., pp. 199-206 (World Scientific Publishing Company, 2011) (also arXiv:1006.2223 [physics.optics]).
25. E. Sorokin and I. T. Sorokina "Ultrashort-pulsed Kerr-lens modelocked Cr:ZnSe laser," paper CF1.3-WED at CLEO/Europe 2009.

1. Introduction

Broadband solid-state and fiber lasers have become promising tools for optical metrology, spectroscopy, environment and industrial monitoring including trace gas detection. Combination of broad smooth spectra with diffraction-limited brightness inherent in such lasers is especially important for high-sensitivity spectroscopic applications. Recent availability of these femtosecond sources, especially those operating in the finger-print region of molecular vibrations at/above 2 μm, enables novel spectroscopic approaches, which allow achieving simultaneously high resolution and record sensitivity at very short recording times. In comparison to LEDs and lamp sources, the femtosecond sources offer higher spectral brightness, permitting more rapid measurements in the broader spectral range, covering several absorption lines simultaneously.

One of the possible implementations of laser spectroscopy is the intracavity absorption spectroscopy allowing direct measurement of important molecular gases with high resolution and good signal-to-noise ratio [1–5]. Progress in development of broadband solid-state oscillators operating in the mid-IR [6], where there is a strong atmospheric absorption, as well as of fiber lasers [7–9], covering the overtone absorption lines of a number of important gases makes the intracavity technique to be of special interest for trace gas analysis applications. At the same time, advancement of the femtosecond oscillators towards mid-IR brings them into the wavelength regions, where the atmosphere itself becomes a major absorber inside the oscillator. The issues of operation stability, spectrum and pulse deformation become important, whenever these sources are to be used for quantitative spectroscopic measurements or ultrashort-pulse applications.

As it was observed in Cr:ZnSe and Cr:YAG femtosecond lasers [10–12], the spectral signatures from the absorption lines look differently, when an absorber is inside the cavity of a

#149532 - $15.00 USD Received 20 Jun 2011; revised 28 Jul 2011; accepted 5 Aug 2011; published 22 Aug 2011

mode-locked oscillator or when it is introduced after the output mirror. For the conventional femtosecond oscillator, the spectral signal induced by an intracavity absorption line followed an associated index of refraction of absorber and was significantly enhanced compared to the linear absorption signal from the same optical path. This observation stimulated research aimed at developing the theory of the soliton absorption spectroscopy [13]. This theory is based on the soliton perturbation theory and applies to both, passively modelocked femtosecond pulse oscillators with intracavity absorbers and soliton propagation in fibers with narrowband impurities. The main condition underlying the theory is that the soliton propagation conditions are realized, i.e. the net-group-delay dispersion (GDD) is anomalous (anomalous dispersion regime, ADR) and the femtosecond pulse is chirp-free.

During the last five years, rapid progress has been achieved in the theoretical studies and experimental realization of the alternative regime of ultrashort pulse generation using the net-normal GDD. Such a regime (normal dispersion regime, NDR) has been realized in chirped-pulse solid-state oscillators (CPOs) [14] and all-normal-dispersion (ANDi) fiber lasers [15]. The NDR possess important advantages: energy scalability [16], and flattened spectrum covering the gain band - hence, making this regime more and more employed for generation of high energy pulses and frequency combs. Extension of intracavity absorption techniques to the NDR is therefore of special interest for trace gas analysis and other applications. The issue at the core of this study is that the pulse developing in the NDR is strongly chirped and corresponds to the so-called chirped dissipative soliton (CDS) [16]. Hence, the theory of Ref. [13] cannot be extended to the NDR in a straightforward way. It is the purpose of this paper to develop an analytical theory of dissipative soliton absorption spectroscopy in the NDR.

In this paper we consider the effect of a narrowband absorption on the CDS developing in the NDR. The analytical treatment is based on the perturbation analysis of the approximated CDS solutions of the complex cubic-quintic nonlinear Ginzburg-Landau equation (CNGLE). We find that the spectrum acquires signatures, which follow the associated refractive index of absorber and scale with the soliton wavenumber, as it takes place in the anomalous dispersion regime. At the same time, the perturbation exhibits resonance enhancement when approaching the CDS spectrum edges. Further, the narrow line may cause asymmetric distortion of the pulse spectrum as a whole, which, however, does not affect recognition of individual signals from the lines. The analytical theory is confirmed by numerical simulations and by experimental data from a chirped-pulse Cr:ZnSe laser. Finally, we provide quite general expressions that allow measuring the absorption from signal amplitude using only experimental observables such as dispersion and spectrum width.

2. Model

Our approach is based on description of the ultrashort pulse developing in an oscillator (solid-state or fiber) represented by a complex cubic-quintic nonlinear Ginzburg-Landau equation (CNGLE) [17]:

$$\frac{\partial a(z,t)}{\partial z} = -\sigma a(z,t) + (\alpha + i\beta)\frac{\partial^2}{\partial t^2}a(z,t) + [\kappa(1-\zeta P(z,t)) - i\gamma]P(z,t)\,a(z,t) + \hat{\Pi}[a], \quad (1)$$

where the non-dissipative factors are the self-phase modulation (SPM) with the inverse power coefficient γ and the GDD with the coefficient β ($\beta > 0$ corresponds to the NDR); and the dissipative factors are the net-loss (i.e. the unsaturable loss minus the gain saturated by the energy $E \equiv \int_{-\infty}^{\infty} |a|^2\, dt$) with the coefficient σ, the frequency filtering with the squared inverse bandwidth α (e.g. gain bandwidth), the self-amplitude modulation (SAM; κ is the inverse loss saturation power multiplied by the saturable loss coefficient), and the saturation of SAM with the inverse power coefficient ζ. In Eq. (1) z is the cavity round-trip number for a distributed

#149532 - $15.00 USD Received 20 Jun 2011; revised 28 Jul 2011; accepted 5 Aug 2011; published 22 Aug 2011

oscillator, t is the local time, and $P \equiv |a|^2$ is the instant power. The operator $\hat{\Pi}$ describes a perturbation caused by the frequency- dependent losses.

The general solution of Eq. (1) is unknown, but the approximate CDS solution can be obtained on the basis of the adiabatic approximation and the method of stationary phase [18, 19]. In the time-domain, the CDS can be expressed in the following form:

$$a(z,t) = \sqrt{P(t)} \exp\left[i\left(\phi(t) - qz\right)\right], \tag{2}$$

where $\phi(t)$ is the phase and q is the wavenumber, i.e. the phase produced by slip of the carrier phase in relation to the slowly varying envelope. Substitution of Eq. (2) in Eq. (1) allows obtaining the approximated analytical solution in the spectral domain (calculations are documented in [20, 21]):

$$e(\omega) \approx \sqrt{\frac{6\pi B}{\Xi^2 + \omega^2}} \exp\left[\frac{3iBC\omega^2}{2\left(\Xi^2 + \omega^2\right)\left(\Delta^2 - \omega^2\right)} - \frac{i\pi}{4}\right] H\left(\Delta^2 - \omega^2\right), \tag{3}$$

where $e(\omega)$ is the spectral amplitude, H is the Heaviside function, power is normalized to ζ, and time is normalized to $\sqrt{\alpha\zeta/\kappa}$. The normalized parameters become

$$\begin{gathered} q = P_0 = \frac{3}{4}\left(1 - \frac{C}{2} \pm \sqrt{\left(1 - C/2\right)^2 - 4A}\right), \\ \Delta^2 = Cq, \\ \Xi^2 = (1+C)C - \frac{5}{3}\Delta^2, \\ T = \frac{3CD}{\Delta^2(\Delta^2 + \Xi^2)}, \end{gathered} \tag{4}$$

Here Δ is the normalized half-width of the spectrum, T is the characteristic CDS temporal width, and P_0 is the normalized peak power, where two signs correspond to the so-called positive and negative branches. The solution has a shape of the Lorentz function truncated at $\pm\Delta$ [18]:

$$p(\omega) \equiv |e(\omega)|^2 \approx \frac{6\pi B}{\Xi^2 + \omega^2} H\left(\Delta^2 - \omega^2\right). \tag{5}$$

The positive branch CDS has non-trivial limit $A \to 0$ (the vacuum stability limit of the CNGLE), higher energy, and broader spectrum, while the negative branch CDS has almost a flat-top spectrum, corresponding to $\Delta^2 \ll \Xi^2$. The oscillator parameters enter the solution as dimensionless coefficients

$$A \equiv \frac{\zeta\sigma}{\kappa},\ B \equiv \frac{\gamma}{\zeta},\ C \equiv \frac{\alpha\gamma}{\beta\kappa},\ D \equiv \frac{\gamma}{\kappa}. \tag{6}$$

The stability of the approximated solution [Eq. (3)] has been explored in Refs. [19, 22, 23] on the basis of extensive numerical simulations. It has been shown that the CDS corresponding to Eq. (3) is stable in the presence of gain saturation, i.e. when σ-parameter in Eq. (1) is energy-dependent. It has been also demonstrated that a distortion of the CDS spectral profile can develop at the singularity points $\omega = \pm\Delta$ [23], where the resonant amplification of perturbations is possible (see Fig. 4,*a* below and [24]). With these limitations in mind in the rest of this section we apply the perturbation approach to the analytical solution [Eq. (3)].

As the perturbation source, we consider a superposition of N weak and narrow absorption lines with causal Lorentz profiles [13]:

$$\hat{\Pi}[a(z,t)] \propto \sum_l \varepsilon_l \Omega_l \int_{-\infty}^{t} e^{-(\Omega_l - i\omega_l)(t-t')} a\left(z,t'\right) dt', \tag{7}$$

#149532 - $15.00 USD Received 20 Jun 2011; revised 28 Jul 2011; accepted 5 Aug 2011; published 22 Aug 2011

where $\varepsilon_l < 0$ are the loss coefficients, ω_l are the resonant frequencies, and Ω_l are the bandwidths corresponding to each absorption line.

By analogy to [13], we define $f(t)\exp(-iqz)$ as a perturbation signal with an assumption of its phase-matching to the soliton by setting the propagation wavenumber of the perturbation equal to q [17]. Substituting $a'(z,t) = a(t) + f(t)\exp(-iqz)$ into Eq. (1), and linearizing with respect to f, we obtain

$$\begin{aligned} i\left(\sigma f(t) - \alpha\frac{\partial^2 f(t)}{\partial t^2}\right) + qf(t) + \beta\frac{\partial^2 f(t)}{\partial t^2} = i\hat{\Pi}[a(t)] + \\ + i\kappa\left[a(t)^2 f^*(t) + 2|a(t)|^2 f(t) - \zeta|a(t)|^2\left(2a(t)^2 f^*(t) + 3|a(t)|^2 f(t)\right)\right] + \\ + \gamma\left(a(t)^2 f^*(t) + 2|a(t)|^2 f(t)\right), \end{aligned} \tag{8}$$

where f^* is the complex conjugate perturbation amplitude.

Simple analytical form of solution [Eq. (3)] suggests developing the perturbation theory in the spectral domain. Then the perturbation [Eq. (7)] takes the form

$$\Pi(\omega) \equiv \sum_{l=1}^{N} \varepsilon_l \frac{1 - i(\omega - \omega_l)/\Omega_l}{1 + (\omega - \omega_l)^2/\Omega_l^2} \tag{9}$$

and the Eq. (8) becomes

$$f(\omega)\left[i\left(\sigma + \alpha\omega^2\right) + q - \beta\omega^2\right] = ie(\omega)\sum_{l=1}^{N}\varepsilon_l\left[1 + \frac{i(\omega - \omega_l)}{\Omega_l}\right]^{-1} + \tag{10}$$

$$+\frac{i}{2\pi}\int_{-\infty}^{\infty} d\omega'\left[\Upsilon_1(\omega-\omega')f^*(\omega') + \Upsilon_2(\omega-\omega')f(\omega') + \Upsilon_3(\omega-\omega')f^*(\omega') + \Upsilon_4(\omega-\omega')f(\omega')\right],$$

where Υ-terms in the convolution represent the nonlinear terms of CNGLE. $\Upsilon_1$and Υ_3 (i.e. images of $(\kappa - i\gamma)a^2$ and $-2\kappa\zeta|a|^2a^2$, respectively) can be found by means of the stationary phase method like Eq. (3):

$$\Upsilon_1 \approx B\left(\frac{1}{D} - i\right)\sqrt{\frac{3\pi B(\Delta^2 - \omega^2)}{C(\Xi^2 + \omega^2)}}\exp\left[\frac{3iBC\omega^2}{4(\Xi^2 + \omega^2)(\Delta^2 - \omega^2)} - \frac{i\pi}{4}\right]H\left(\Delta^2 - \omega^2\right), \tag{11}$$

$$\Upsilon_3 \approx -\frac{2B}{D}\sqrt{\frac{3\pi B}{\Xi^2 + \omega^2}}\frac{\left(\Delta^2 - \omega^2\right)^{\frac{3}{2}}}{C^{3/2}}\exp\left[\frac{3iBC\omega^2}{4(\Xi^2 + \omega^2)(\Delta^2 - \omega^2)} - \frac{i\pi}{4}\right]H\left(\Delta^2 - \omega^2\right). \tag{12}$$

To find Υ_2 and Υ_4 (images of $2(\kappa - i\gamma)|a|^2$ and $-3\kappa\zeta|a|^4$, respectively), one can use the approximated expression for the CDS power profile: $P(t) \approx P_0\mathrm{sech}(t/T)^2$, which becomes exact in the $\zeta \to 0$ limit [16]. Then

$$\Upsilon_2 \approx 2B\left(\frac{1}{D} - i\right)P_0\pi T^2\omega\,\mathrm{csch}\left(\frac{\pi\omega T}{2}\right), \tag{13}$$

$$\Upsilon_4 \approx -\frac{B}{2D}P_0^2\pi T^2\omega\left(4 + T^2\omega^2\right)\mathrm{csch}\left(\frac{\pi\omega T}{2}\right). \tag{14}$$

Equation (10) is the Fredholm integral equation of the second kind. Its solution can be obtained iteratively in the form of the Neumann series, in analogy to [13]. The zero-order approximation only accounts for the contribution of the first term in the right-hand side of Eq. (10). For weak

#149532 - $15.00 USD Received 20 Jun 2011; revised 28 Jul 2011; accepted 5 Aug 2011; published 22 Aug 2011

absorption lines $|\varepsilon| \ll 1$ sufficiently far from the edges of the spectrum $\Omega_l^2 \ll \Delta^2$ the perturbed spectral power profile $p'(\omega) = |e(\omega) + f(\omega)|^2$ can be expressed as [21]

$$p'(\omega) \approx \frac{6\pi B}{\Xi^2 + \omega^2} H\left(\Delta^2 - \omega^2\right) \left[1 + \frac{2C}{B} \sum_{l=1}^{N} \frac{\varepsilon_l}{\Delta^2 - \omega_l^2} \frac{(\omega - \omega_l)/\Omega_l}{1 + (\omega - \omega_l)^2 / \Omega_l^2}\right], \tag{15}$$

where we also assumed low saturation per pass ($\sigma \ll 1$) and prevalence of non-dissipative factors such as SPM and GDD over dissipative such as SAM and frequency filtering: $\kappa \ll \gamma$, $\kappa\zeta \ll \gamma^2$, and $\alpha \ll \beta$. These assumptions are well justified for most NDR solid-state oscillators.

For stronger absorption lines ($|\varepsilon| \gtrsim 1$) or lines near the edges of the spectrum ($\Omega_l^2 \approx \Delta^2$) we can obtain corrections to Eq. (15) in the form of Neumann series solution of Eq. (10) under the above assumptions $\sigma \ll 1$, $\kappa \ll \gamma$, $\kappa\zeta \ll \gamma^2$, $\alpha \ll \beta$, and

$$\int_{-\infty}^{\infty} d\omega' \Upsilon_1\left(\omega - \omega'\right) f^*(\omega') = \int_{-\infty}^{\infty} d\omega' \Upsilon_2\left(\omega - \omega'\right) f(\omega'). \tag{16}$$

The resulting iterative solution for the spectral perturbation is

$$\begin{aligned} f_n(\omega) &= S(\omega) + \frac{3T^2}{2\left(1 - \omega^2/\Delta^2\right)} \int_{-\infty}^{\infty} d\omega' \left(\omega - \omega'\right) \operatorname{csch}\left(\frac{\pi T}{2}\left(\omega - \omega'\right)\right) f_{n-1}(\omega'), \\ S(\omega) &= \frac{iC}{B\left(\Delta^2 - \omega^2\right)} e(\omega)\Pi(\omega), \\ f_0(\omega) &= S(\omega). \end{aligned} \tag{17}$$

In the general case, we should include all convolutions in Eq. (10) which results in two interrelated iterative equations for f_n and f_n^*, with $f_0 = S$ and $f_0^* = S^*$.

It should be noted at this point that zero-order solution in the form of Eq. (15) is linear with respect to the individual absorption lines. It is therefore equally applicable to the dense line groups like e.g. Q-branch, and inhomogeneously broadened lines like e.g. Gaussian and more general Voigt profiles, as they can be represented as a superposition (convolution) of individual narrow Lorentzians. Since the spectral signatures trace the index of refraction of an absorber, the shape of this trace depends on the profile of an absorption line.

Another interesting property of the solution [Eq. (15)] is its temporal structure. The perturbed field $a'(t)$ is by construction a sum of an unperturbed pulse $a(t)$ and the perturbation $f(t)$, which in the zero-order approximation is a time-domain image of the $S(\omega)$ function in Eq. (17). In the vicinity of a narrow resonance $\omega \approx \omega_l$ both $e(\omega)$ and $\Delta^2 - \omega^2$ are slowly varying, so that the perturbation signal becomes $S(\omega) \propto i\Pi(\omega)$, i.e. a sum of imaginary Lorentzians. Their time-domain images are decaying exponentials, so that the perturbation $f(t)$ is a superposition of exponential tails at frequencies ω_l with time constants $1/\Omega_l$. This property holds for conventional soliton [13] as well.

In the next sections we shall concentrate on the zero-order solution [Eq. (15)]: illustrate its properties and numerically explore limitations of applicability, as well as provide experimental verification.

3. Results and discussion

To illustrate the results of the previous section, we will perform calculations for a model system with parameters approaching those of a typical Cr:ZnSe oscillator. Table 1 summarizes the parameters, used for the simulations.

#149532 - $15.00 USD Received 20 Jun 2011; revised 28 Jul 2011; accepted 5 Aug 2011; published 22 Aug 2011

Table 1. Basic Parameters for Numerical Simulations

α, fs^2	β, fs^2	κ	ζ	σ	$A \equiv \frac{\zeta\sigma}{\kappa}$	$B \equiv \frac{\gamma}{\zeta}$	$C \equiv \frac{\alpha\gamma}{\beta\kappa}$	$D \equiv \frac{\gamma}{\kappa}$
16	250	0.04γ	0.2γ	2.5×10^{-4}	1.25×10^{-3}	5	1.6	25

The unperturbed analytical spectra [Eq. (5)] corresponding to the positive (solid) and negative (dashed) branches of CDS are shown in Fig. 1. The properties of these solutions are reviewed in [16, 19, 22]. The negative branch CDS exists in a broader range of GDD and its lower bandwidth Δ would even stronger perturbation signal Eq. (13). The positive branch CDS has a broader spectrum and is energy scalable (in the sense of [16]). Below, we shall consider the negative branch CDS without loss of generality.

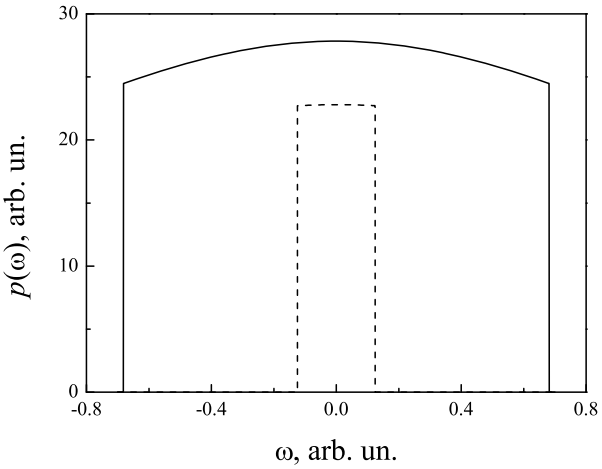

Fig. 1. The unperturbed CDS spectra corresponding to Eq. (5) and to parameters in the Table 1. The positive (negative) branch is shown by a solid (dashed) line.

The central part of the CDS spectrum perturbed by a single absorption line with ε_1 =-0.0025, ω_1 =0 (all frequencies are measured relative to the CDS carrier), and Ω_1 =1 GHz is shown in Fig. 2. The spectrum shown by the red solid curve corresponds to the zero-order approximation in Eq. (17). Note that the perturbed power spectrum follows an associated index of refraction of the absorber, like it does in the case of a Schröinger soliton [13].

Open black circles in Fig. 2 show the power spectrum in the first-order approximation in Eq. (17) under the assumption Eq. (16) while blue crosses show the same approximation but without the assumption Eq. (16). One can see that all profiles coincide within a spectral scale comparable with Ω_l, and as a result, Eq. (15) gives a perfect local approximation for the exact solution.

Simultaneously, the contribution of the convolutions in Eq. (10) results in a large-scale perturbation of the CDS spectrum (compare red curve in Fig. 3 with black open circles and blue crosses). If the assumption Eq. (16) is abandoned (blue crosses), the large-scale perturbations occur mainly on the high-frequency side of the spectrum.

Figure 3 (circles and crosses) demonstrates that the spectrum edges are most sensitive to the perturbations (compare with the results of [16, 23, 24]), which grow due to the resonant term in Eq. (17). Such enhancement can be useful for additional increase of sensitivity for the weak absorption lines as it is shown in Fig. 4. Figure 4, *a* demonstrates the contribution of several identical absorption lines located at the different position $\omega_l > 0$. The contribution is calculated

#149532 - $15.00 USD Received 20 Jun 2011; revised 28 Jul 2011; accepted 5 Aug 2011; published 22 Aug 2011

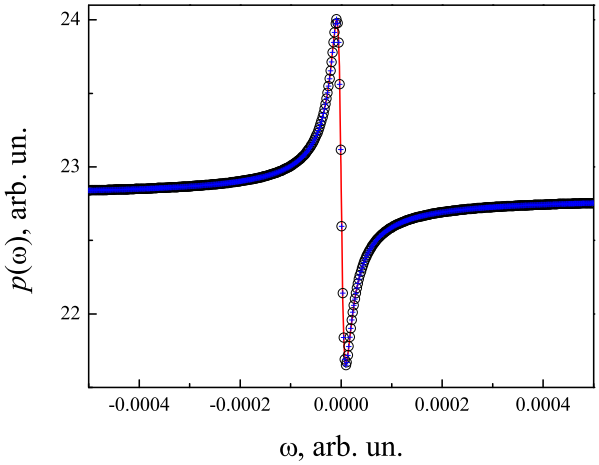

Fig. 2. The perturbed CDS spectra for the negative branch CDS and the parameters of Table 1. A single absorption line with ε_1 =-0.0025, ω_1 =0, and Ω_1 =1 GHz contributes. Solid red curve corresponds to contribution of $f_0(\omega)$ in Eq. (17), open black circles correspond to contribution of $f_1(\omega)$ under the assumption Eq. (16), and blue crosses show $f_1(\omega)$ without the assumption Eq. (16).

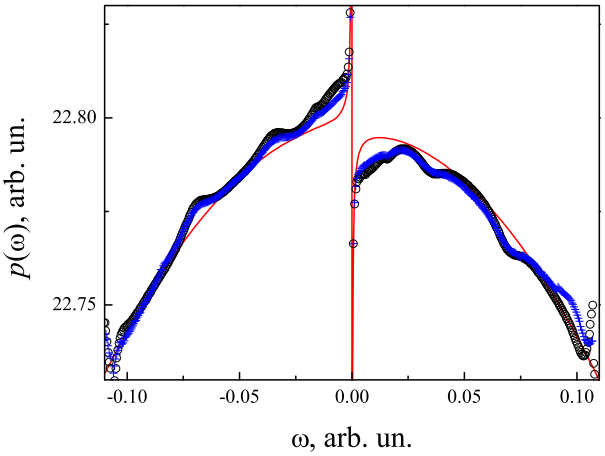

Fig. 3. The scaled-down perturbed CDS spectra corresponding to those in Fig. 2.

#149532 - $15.00 USD Received 20 Jun 2011; revised 28 Jul 2011; accepted 5 Aug 2011; published 22 Aug 2011

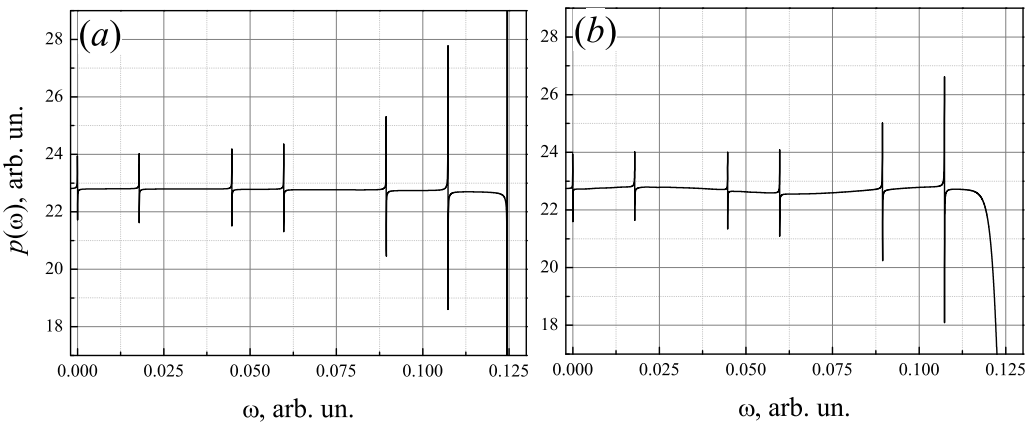

Fig. 4. Perturbed spectra obtained from the zero-order approximation of Eq. (17) *(a)*, and from the numerical simulations of the Eq. (1) *(b)*. Six identical absorption lines are considered, with ε_l =-0.0025 and Ω_l =1 GHz. Simulation parameters correspond to those in Table 1.

in the zero-order approximation of Eq. (17). The enhancement of the perturbation amplitude near the spectrum edge is clearly visible. The giant jump at the spectrum edge $\omega = \Delta$ results from a singularity in Eq. (17) and is beyond the used approximations.

4. Numerical and experimental verification

For verification of the analytical results, the numerical simulations of Eq. (1) perturbed by Eq. (9) have been performed on a basis of the symmetrized split-step Fourier method. The time step equals to 2.5 fs, the time window equals to ≈10 ns (2^{22} mesh points), and the cavity round trip is divided into 10 sub-steps. Other parameters correspond to those in Table 1. The simulation time is chosen to $>$ 10000 round-trips to ensure reliable convergence. As the initial condition, we used a 250-fs long sech-shaped seed pulse without chirp and with $10^{-10}/\gamma$ peak power.

A representative numerical spectrum is shown in Fig. 4, *b*. As was pointed out previously [19], the numerical CDS spectrum has somewhat smoothed edges (this also corresponds to the experiment) but its basic features are perfectly described by the approximated analytical solution. The structure of numerical spectrum agrees with the analytical, which is obtained in the zero-order approximation of Eq. (17), and he enhancement of perturbation near the spectrum edge is clearly visible. At the same time, there are two minor differences between the spectra. The first difference is the large-scale perturbation of the spectrum envelope as a whole. The source of this effect can be identified with the contribution of higher-order terms in Eq. (17) resulted from the convolutions in Eq. (10) (see Fig. 3). The remarkable feature of the large-scale perturbation is that it appears exclusively in the NDR and within the region of $\omega > \omega_l$ (Figs. 4, *b*; Fig. 5). The second difference is the increasing up-down asymmetry of the numerical perturbation spikes near the spectrum edge. When the absorption line is located right at the spectrum edge, the asymmetry becomes so high that the perturbation is observed only as a gap (right and left sides of the spectrum in Fig. 5). We attribute this effect to the breaking of the approximations at the spectrum edge.

As experimental verification we consider the chirped-pulse operation of a Kerr-Lens mode-locked Cr:ZnSe laser [25]. The laser operated at 91.6 MHz repetition rate at open air in the vicinity of zero intracavity dispersion. Besides the 4-mm long active element, the cavity in-

#149532 - $15.00 USD Received 20 Jun 2011; revised 28 Jul 2011; accepted 5 Aug 2011; published 22 Aug 2011

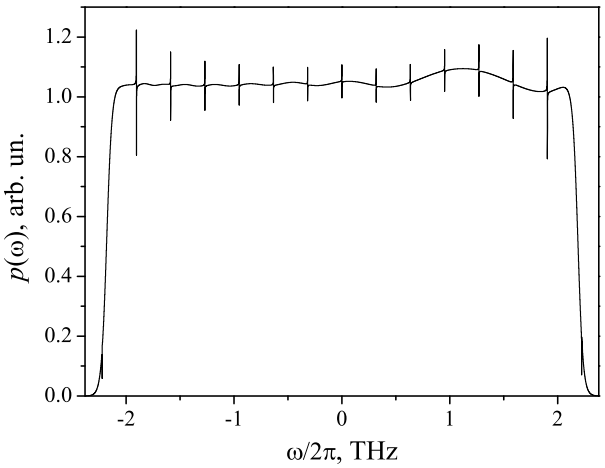

Fig. 5. Numerical spectrum for ε_l =-0.0025 and Ω_l =1 GHz and another parameters described in Table 1.

cluded a 6.3-mm thick YAG plate, 5 highly-reflective mirrors and an output coupler. The overall round-trip dispersion is computed using the known material and mirror coating data and is shown in Fig. 6, *a*. Since the zero-dispersion wavelength at 2450 nm coincided with the gain maximum of the material, it was possible to operate the laser in both, soliton and chirped-pulse regimes [25]. In the first case, the laser spectrum was centered near 2500 nm, and was in the region of the anomalous dispersion. The pulses of ≈100 fs duration did not carry any significant chirp, and the spectrum contained all the typical features of intracavity absorption as described in Ref. [13]. This regime was rather unstable because of the fast increase of water vapor absorption beyond 2500 nm. In the second regime, the laser operated with its spectrum shifted towards 2300 nm, emitting strongly chirped pulses of about 1 ps duration (Fig. 6, *b*). This regime was stable with the main part of the spectrum well in the normal dispersion region. At 91 MHz repetition rate the average output power was 170 mW through the 1.8% output coupler, corresponding to 1.9 nJ output pulse energy or 100 nJ intracavity pulse energy.

Figure 6, *a* clearly demonstrates typical dispersion-like features superimposed on the smooth pulse spectrum, as predicted by the solution Eq. (15). For quantitative analysis, it is convenient to single out the modulation part of the solution [Eq. (15)] and revert the normalizations:

$$\frac{p'(\omega)}{p(\omega)} = 1 + \frac{1}{\beta\Delta^2}\sum_{l=1}^{N}\frac{2\varepsilon_l}{1-\omega_l^2/\Delta^2}\frac{(\omega-\omega_l)/\Omega_l}{1+(\omega-\omega_l)^2/\Omega_l^2}, \tag{18}$$

where now the observables β and Δ can be directly accessed as the group delay dispersion and spectrum half-width in circular frequency units, respectively. Recalling that $q=\beta\Delta^2$ is the chirped soliton wavenumber, we see that this result has the same form as Eq. (17) in Ref. [13]. The principle difference lies with the frequency dependence of the modulation depth. While the chirped soliton exhibits resonance enhancement towards spectrum edges as $(1-\omega_l^2/\Delta^2)^{-1}$, the modulation depth for conventional soliton would decrease as $(1+\omega_l^2T_0^2)^{-1}$ (Eq. (14) in Ref. [13]).

Applying numerical values to the spectrum in Fig. 6, *a* can not be performed as straitforwardly as in [13], because the pulse spectrum strongly deviates from the symmetric profile with cut wings, required by the expression (15) due to the large third-order dispersion (51000 fs^3 at 2400 nm). Detailed description of the third-order dispersion influence on dissipative soliton is beyond the scope of this work, but for our purposes it is sufficient to estimate the 2Δ parameter,

#149532 - $15.00 USD Received 20 Jun 2011; revised 28 Jul 2011; accepted 5 Aug 2011; published 22 Aug 2011

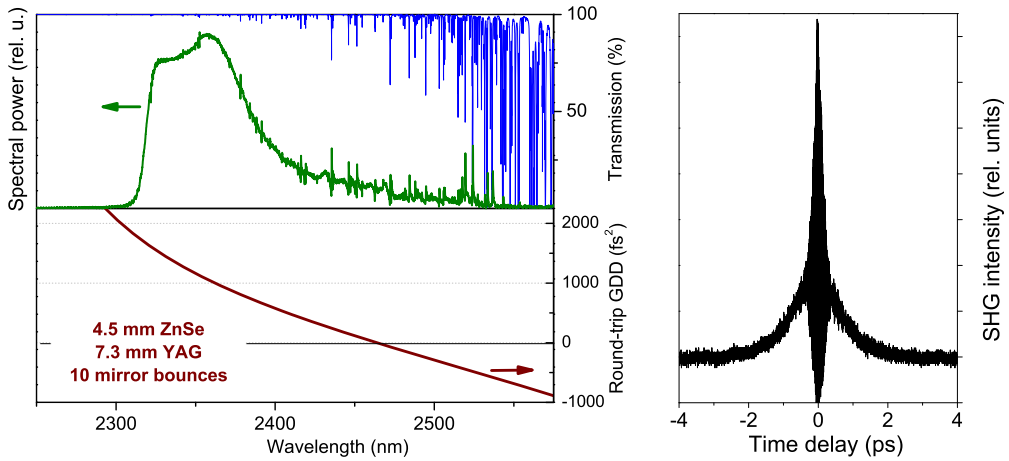

Fig. 6. Kerr-lens mode-locked Cr:ZnSe laser in normal dispersion regime. (a) Round-trip dispersion and output spectrum (note that the GDD curve presented here corrects the data of Ref. [25] by accounting for the mirrors' dispersion.) The round-trip transmission of the atmosphere (HITRAN) is shown in blue. (b) The autocorrelation trace of the chirped pulse.

for which we take the full width at half maximum $2\Delta = 70 \pm 5$ nm. Taking $\beta = 1100 \pm 100$ fs^2 in the central part of the spectrum we obtain $\beta\Delta^2 = 0.155 \pm 0.025$, i.e. (6.5 ± 1)-fold enhancement of the intracavity modulation with respect to the absorption peak. Fig. 7 shows the expanded central part of the measured spectrum along with the absorption lines, calculated from HITRAN database, assuming the measured conditions of 30±2% relative humidity and 23.5 ± 0.5 °C at the time of experiment. The observed 6-fold enhancement of the modulation amplitude is in a very good agreement with the estimation, well within the uncertainty in β and 2Δ parameters.

Finally, it is instructive to express the modulation amplitude $|\varepsilon_l/q|$ at $\omega_l = \omega \pm \Omega_l$ through the observable parameters, such as spectrum FWHM $\Delta\nu$ and round-trip GDD β, peak absorption $\chi_l L = 2\varepsilon_l$ over the round-trip intracavity absorber path length L, equal to the double resonator length in our case:

$$\left|\frac{\varepsilon_l}{q}\right| = \frac{\chi_l L}{2}\frac{1}{\beta\Delta^2} = \chi_l L \frac{0.0507}{\beta(\Delta\nu)^2}. \tag{19}$$

The numerical coefficient $1/2\pi^2 \approx 0.05066$ in the numerator differs only by a factor of 1.6 from the corresponding coefficient $\operatorname{arccosh}(3)^2/\pi^4 \approx 0.0319$ obtained for a chirp-free conventional soliton [13]. The good agreement with the experiment suggests also that this relation is quite tolerant to the presence of higher-order dispersion, as already observed in [13], and to the deviation of the the spectrum from analytical expression.

The fact that the analytical form and numerical expressions for the intracavity signal in so different regimes of operation coincide within a small correction factor allows making a more general statement. In particular, we suggest that the spectral modulation caused by a narrow-band inracavity absorber in *any* passively modelocked laser has a form of the associated index of refraction, with the modulation amplitude at the spectrum center depending only on the absorber coefficient, pulse spectrum width, and GDD parameter. It is given by the expression (19) with a correction factor, close to unity. At the same time, the behavior of modulation amplitude at the spectrum wings does depend upon the spectrum shape and chirp.

#149532 - $15.00 USD Received 20 Jun 2011; revised 28 Jul 2011; accepted 5 Aug 2011; published 22 Aug 2011

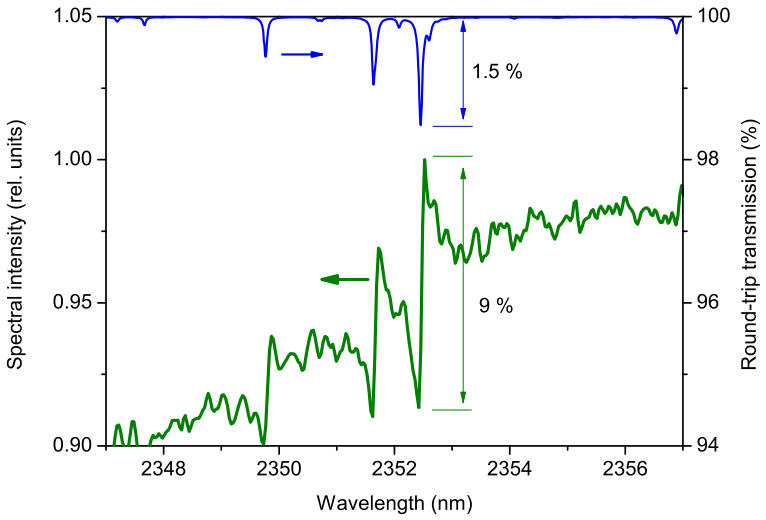

Fig. 7. Modulation signal due to the atmospheric water-vapour lines in the Cr:ZnSe laser, central part expanded. The percentage marks show the peak line absorption ($2\varepsilon_l L$) and signal amplitude ($2\varepsilon_l/\beta\Delta^2$) between the peaks at $\omega = \Omega_l \pm \omega_l$.

Formula (19) also provides means to estimate the energy content of the extended pulse tail in the time domain, discussed in Section 2. Since the time constant of this tail is much longer than the pulse duration, its overlap with the main pulse is negligible. We can therefore assume that the energy content of the tail equals the total energy of the perturbation signal $f(t)$ and calculate the energy fraction within the tail as

$$\frac{E_{tail}}{E_{pulse}} \approx \frac{1}{\beta\Delta^2}\sum_{l=1}^{N}\frac{2\varepsilon_l\cdot\pi}{1-\omega_l^2/\Delta^2} = \frac{0.05}{\beta(\Delta\nu)^2}\sum_{l=1}^{N}\frac{S_l}{1-\omega_l^2/\Delta^2}, \tag{20}$$

where S_l is the integrated absorption of the lth line over the cavity round-trip. Neglecting the enhancement factor $1/(1-\omega_l^2/\Delta^2)$ we finally obtain a practical estimation formula, valid for any passively modelocked laser:

$$\frac{E_{tail}}{E_{pulse}} = (0.04\pm 0.01)\cdot\frac{S}{|\beta|(\Delta\nu)^2}, \tag{21}$$

where S is the total integrated intracavity absorption over the spectrum width $\Delta\nu$.

5. Conclusion

Summarizing, we present an analytical theory of dissipative soliton absorption spectroscopy. We demonstrate that a dissipative soliton formed in a net-normal-dispersion oscillator with a narrowband intracavity absorber acquires spectral features that follow the index of refraction of the absorber. Similarly to the case of soliton absorption spectroscopy in an anomalous dispersion regime [13], we observe over tenfold enhancement of the spectral signal induced by an absorption line on the pulse spectrum in comparison to the conventional absorption signal. The signal enhancement inversely scales with the dispersion and the square of the spectrum width and can be controlled experimentally. In contrast to the soliton absorption spectroscopy in an anomalous dispersion regime, we anticipate resonant enhancement of the modulation signal near the pulse spectrum edges that results in additional signal gain. In the time domain, the

#149532 - $15.00 USD Received 20 Jun 2011; revised 28 Jul 2011; accepted 5 Aug 2011; published 22 Aug 2011

pulse acquires a tail with characteristic time constant defined by the inverse linewidth of the absorber.

The validity of the developed theory is confirmed by results of the numerical simulations and by experimental evidence in a Cr:ZnSe laser oscillator operating in the chirped-pulse regime. The quantitative result and qualitative dependence of the signal on laser parameters are very close to those for the conventional soliton [13] and probably hold for any passively mode-locked laser. The results are particularly interesting for the ultrabroadband femtosecond solid-state and fiber laser sources operating at wavelengths near and above 1.5 μm. They can be used to calculate the influence of the atmospheric absorption on oscillator parameters and for designing sensitive quantitative intracavity measurements.

Acknowledgments

VLK acknowledges the support of the Austrian Fonds zur Föerderung der wissenschaftlichen Forschung (FWF project P20293), ITS acknowledges the support of the Norwegian Research Council (project 191614/V30).

#149532 - $15.00 USD Received 20 Jun 2011; revised 28 Jul 2011; accepted 5 Aug 2011; published 22 Aug 2011